# Transition Control Using Dielectric-Barrier Discharge Actuators

S. Grundmann
Center of Smart Interfaces, Technische Universität Darmstadt, 64287, Germany

**Abstract**

In the present work artificially excited Tollmien-Schlichting waves were cancelled using plasma actuators operated both in continuous and pulsed modes. To achieve this a vibrating surface, driven by an electromagnetic turbulator, was flush-mounted in a flat plate to excite the TS waves. These were amplified by an adverse pressure gradient induced by an insert on the upper wall of the test section. Control plasma actuators positioned downstream of the excitation actuator attenuate the waves by imparting a steady or unsteady force into the boundary layer. In the case with steady actuation the two actuators change the velocity profile of the laminar boundary layer, which then attenuates the waves by itself. In the case of pulsed actuation the actuator creates an unsteady body force to counteract directly the oscillation. As a result the amplitude of the velocity fluctuations at the excitation frequency is reduced significantly in both cases. The principles and the results of the two sets of experiments are presented and discussed.

This manuscript has been published as: Grundmann, S. & Tropea, C. (2009) 'Experimental Damping of Boundary-Layer Oscillatoins using Plasma Actuators' International Journal of Heat and Fluid Flow, *in press*. [11].

## 1 Introduction

In recent years plasma actuators have been studied and applied to a wide range of flow situations. A comprehensive review of these studies will not be given here. However, a review on flow control applications using non-thermal plasma actuators can be found in [13]. While most groups concentrate on the use of plasma actuators for separation control or inducing transition, the TU Darmstadt group (SLA) is singular in its success in delaying transition and suppressing Tollmien-Schlichting (TS) waves as described in [8], [9], [7] and [10]. The investigations presented in the current paper have been performed in an open-circuit wind tunnel. The boundary layer is created on a flat plate of length 1.6m with an elliptical leading edge and an inclinable flap at the trailing edge. To achieve transition at a shorter distance on the plate, an insert is placed on the ceiling of the wind-tunnel test section, creating an adverse pressure gradient of $25Pa/m$. At this position the freestream velocity is set to 9.6m/s. The disturbances leading to the Tollmien-Schlichting waves are acoustically excited using a vibrating surface. A sketch of the experimental setup is shown in Figure 1.

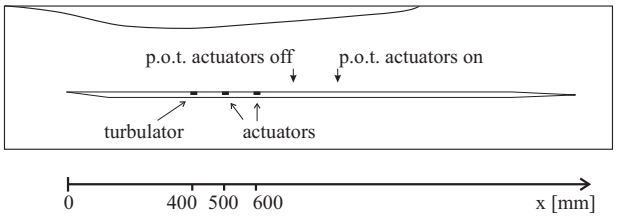


Figure 1: Test section of the wind tunnel (p.o.t.: point of transition)

## 2 Steadily-Operated Plasma Actuators

Initially two plasma actuators are operated in steady mode to dampen the perturbations in the boundary layer. They are positioned at $x = 500mm$ and $x = 600mm$. The plasma actuators used in this work were made of copper tape as electrodes and five layers of Kapton tape as insulation film between the electrodes. The lower covered electrode has a width of $10mm$ and the upper electrode has a width of $2.5mm$. There was no horizontal gap between the electrodes. In the case of steady actuation the actuator was operated at a voltage of $10kV_{pp}$ and at a frequency of $6kHz$. Boundary-layer profile mea-

surements have been performed at 19 downstream positions.

## 2.1 Boundary-Layer Profiles

The following data of a transition-delay experiment using steadily operated plasma actuators was obtained using laser doppler anemometry. Two velocity components, the wall-normal and the wall-parallel, were measured. The oscillations are artificially induced by a vibrating surface. The vibrating surface performs a sinusoidal vertical oscillation and induces single-frequency perturbations clearly recognizable as Tollmien-Schlichting waves in the turbulence profile of Figure 3(d). The results are presented in dimensional form. Due to the incomplete knowledge about the plasma actuator physics, its force distribution and scaling, the results are presented in dimensional form. At this stage, normalization would obscure important information about the range of the actuator effect. The vibrating surface is positioned at $x = 400mm$, which is also the position where the adverse pressure gradient starts. The freestream turbulence in Figure 2(a) has a turbulence level of $T_i = 0.5\%$ [1] and seems to be almost isentropic, at least the horizontal and vertical component. The amplitude of the oscillatory movement of the vibrating surface is so small that the effect of the oscillation cannot be identified immediately above the surface in Figure 2(b). A slight decrease of the maximal turbulence level from $x = 350mm$ and $x = 400mm$ can be found due to the acceleration of the flow field, caused by the insert. More interesting observations can be made in Figure 2(c). Here the profiles were measured directly above the first control actuator. The vertical component has negative values up to $10mm$ in height. A sink-like suction effect downwards towards the actuator is obvious. This suction causes a slight increase of turbulence of the vertical component compared to the uncontrolled case. Already $10mm$ downstream the negative vertical component has turned in slightly increased values compared with the off-case but in higher regions there remains a downward bending of the streamlines, which is indicated by the negative vertical velocity components at $x = 500mm$. The horizontal component is only slightly increased whereas the horizontal fluctuations are more clearly increased. At $x = 550mm$, right between the control actuators, the oscillations of the boundary layer

[1] Here $T_i$ is defined as follows: $T_i = 1/U_\infty \sqrt{1/3(\overline{u'^2} + \overline{v'^2} + \overline{w'^2}}$ with u' and v' as the velocity fluctuations. w' was not measured but assumed to be of the average of u' and v'.

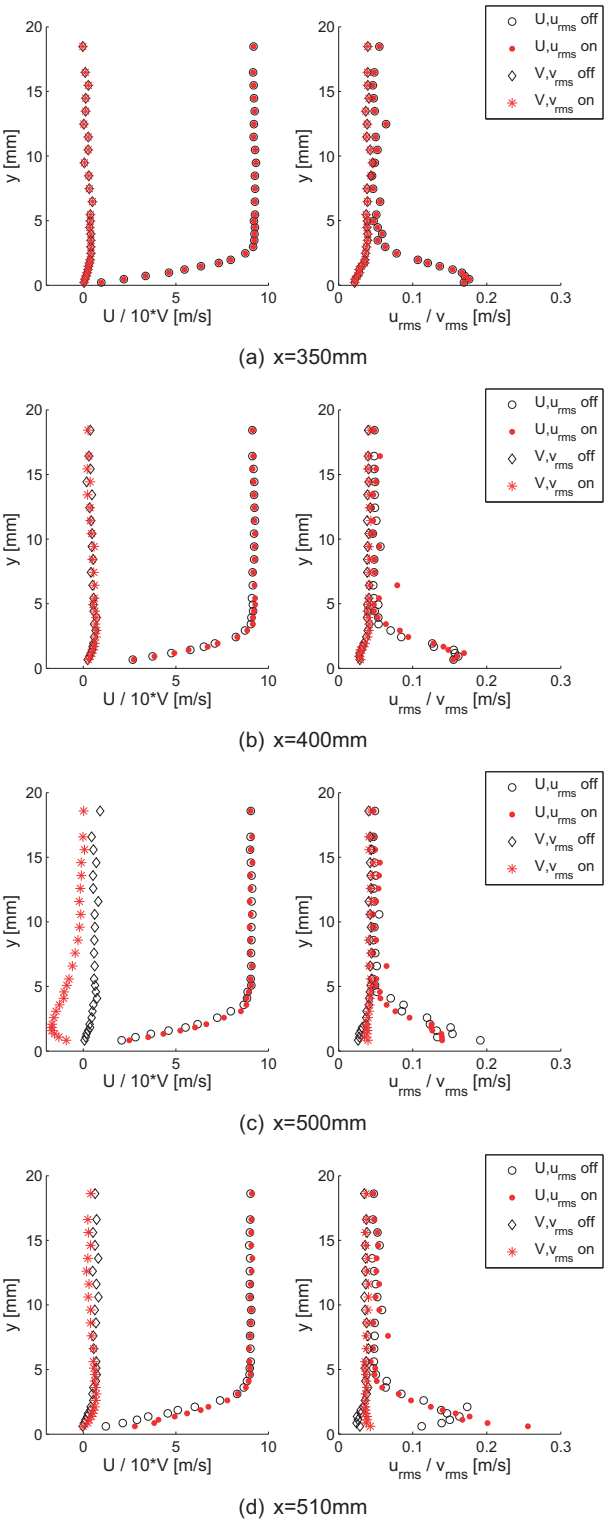


Figure 2: Turbulence and turbulence profiles measured using LDA

are still of such a small amplitude that no considerable difference between the controlled and the uncontrolled case can be seen. Figure 3(b) shows the profiles above the second control actuator. Again the negative vertical velocity components of the case with control stand out. The horizontal velocity fluctuations are increased due to the increased wall shear stress, resulting from the acceleration closed to the wall. Without control the artificially induced perturbations have grown to articulate Tollmien-Schlichting waves. At the next position ($x = 610mm$) the TS waves grow quickly without control actuators turned on and the vertical velocity components of the controlled and the not controlled case start to drift apart. The vertical velocities of the controlled case tend to increase since the profile of a laminar boundary layer with an adverse pressure gradient begins to form. The vertical velocities of the uncontrolled case tend to decrease since a turbulent profile starts to develop. At $x = 610mm$ the most clear TS waves of this experiment can bee seen in Figure 3(c) without control, while the horizontal and vertical fluctuations are still small with the control actuators switched on.

Starting from $x = 700mm$ in Figure 4(a) the uncontrolled boundary layer is in the transition process and a fully developed turbulent boundary layer is being established. This is evident by examining either the mean velocity field, which exhibits a near-wall acceleration or the profile of the velocity fluctuations, which begin to lose the typical shape of TS-waves. Furthermore, as shown in the next section, the shape factor undergoes a strong change at this downstream position, confirming this observation of transition onset. The controlled boundary layer continues developing the features of a laminar boundary-layer profile in an adverse pressure gradient. These features are: Very slow layers right above the surface and a clear inflection point in the profile of the horizontal velocities. At $x = 850mm$ (Figure 4(b)) the fluctuations in the controlled boundary layer grow rapidly and the transition starts also in the case with applied control. At the last measured position both cases show a fully turbulent boundary layer in Figure 4(c) without substantial differences.

## 2.2 Shape Factor

A convenient way to present the results is to plot the shape factor for all downstream positions. The shape factor is defined as the ratio of the displacement thickness $\delta_1$ and the momentum thickness $\delta_2$ of the boundary layer:

$$H_{12} = \frac{\delta_1}{\delta_2}. \qquad (1)$$

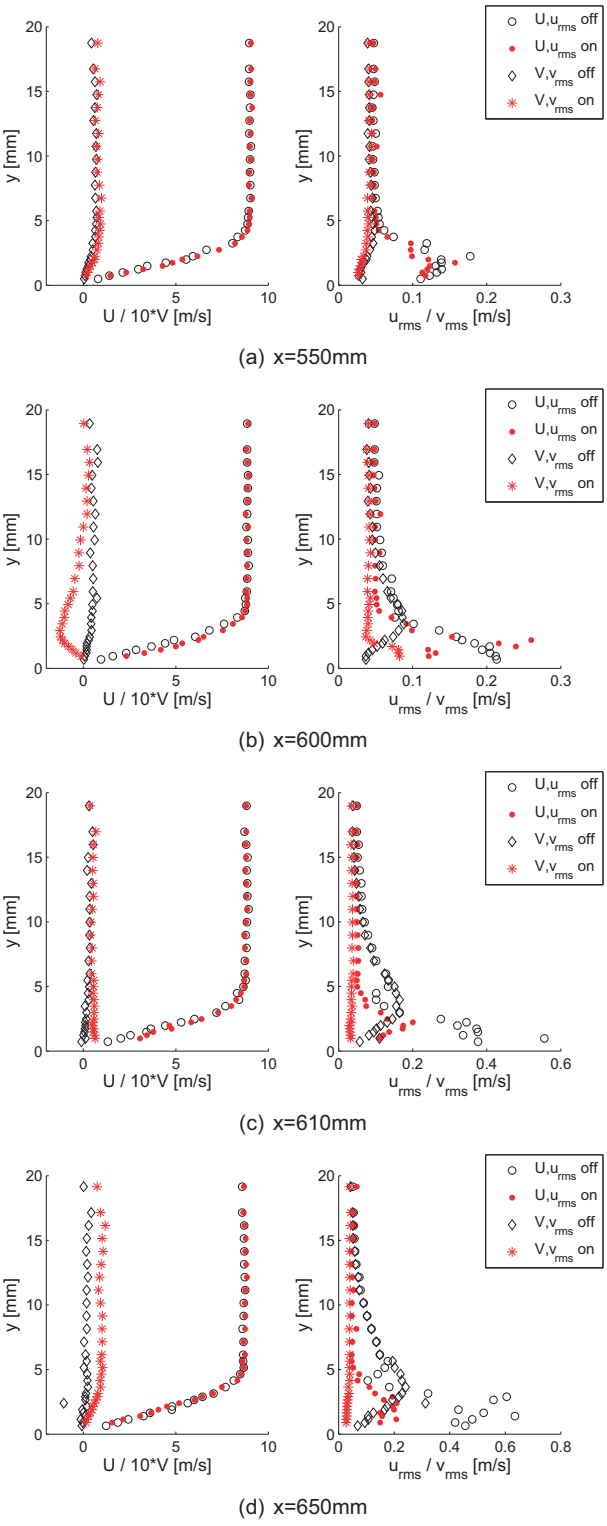


Figure 3: Turbulence and turbulence profiles measured using LDA

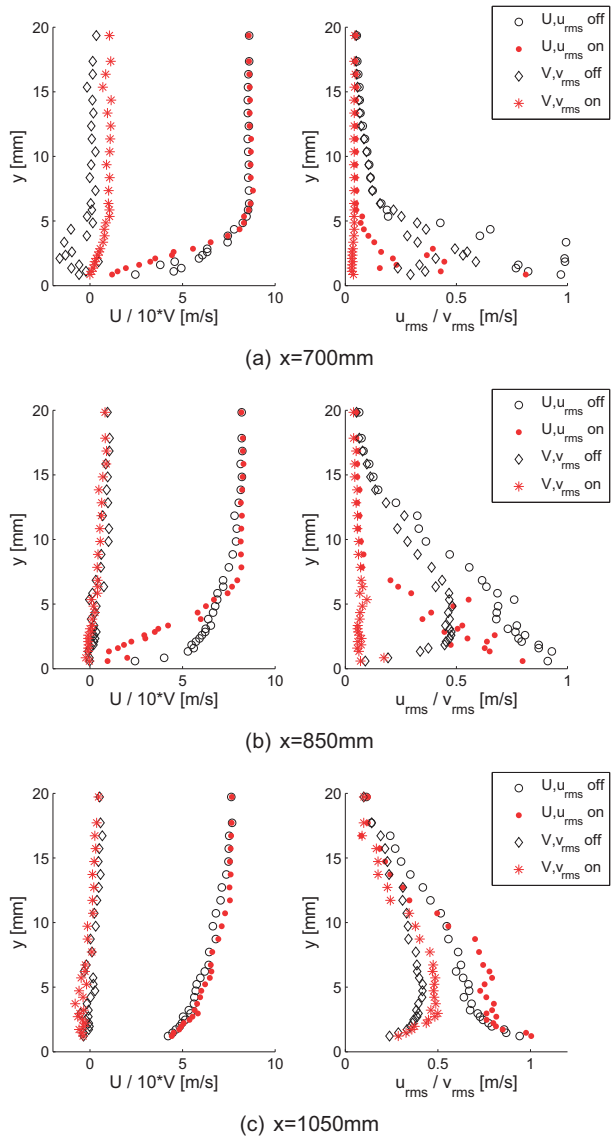


Figure 4: Turbulence and turbulence profiles measured using LDA

The displacement thickness and momentum thickness can be calculated by

$$\delta_1 = \int_0^\infty (1 - \frac{U}{U_\infty})\, dy \quad (2)$$

$$\delta_2 = \int_0^\infty \frac{U}{U_\infty}(1 - \frac{U}{U_\infty})\, dy. \quad (3)$$

The shape factor has a value of $H_{12} = 2.59$ for a Blasius boundary layer, which is a laminar boundary layer with zero pressure gradient. Boundary-layer profiles within an adverse pressure gradient have higher values up to a maximum value of $H_{12} = 4.09$, which is the value of a boundary-layer profile with zero velocity gradient at the wall. Such profiles occur right before a flow separation. Boundary layers with a favorable pressure gradient have lower shape factors, which indicates a more stable profile ($H_{12,min} \approx 2$). Turbulent boundary layers also have low shape factors below 2, usually $H_{12} = 1.4 - 1.6$, which is not to be confused with a laminar boundary layer. If the shape factor of a boundary layer undergoes a sudden drop to lower values without the presence of a favorable pressure gradient, this is clear evidence that the boundary layer has changed from the laminar to the turbulent state. Here those negative slopes of the shape factor diagram have been used to determine a nominal position of transition. Since the slopes of both experiments are moreover parallel it is convenient to compare the horizontal positions where the shape factor has a value of 2 to determine the transition delay. At this point a higher accuracy is not necessary since it is generally understood that transition occurs over a region and not at a single point.

Figure 5 shows a plot of the shape factors of the boundary-layer profiles at all positions with and without control. The circles show the shape factor development of the unstabilized flow and the asterisks show the results of the stabilized flow. It is apparent that the transition could be delayed by approximately $200mm$. The presence of the control actuators is clearly visible in this diagram. The shape factor decreases at $x = 500mm$ and $x = 600mm$ compared with the uncontrolled case due to the acceleration and deformation of the boundary layer for a short distance. The strong increase of the shape factor downstream of the working control actuators shows the presence of the adverse pressure gradient. The mechanism of the damping effect consists of two parts: 1. The body force created by the actuators accelerates the flow and alters the velocity profile to become a more stable profile leading to a much higher critical Reynolds number, which can be

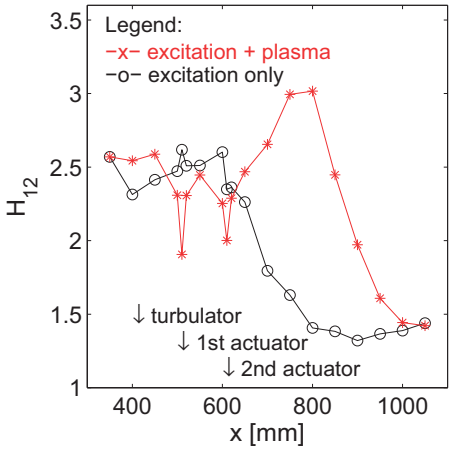


Figure 5: Shape factor development with and without control for the LDA measurements

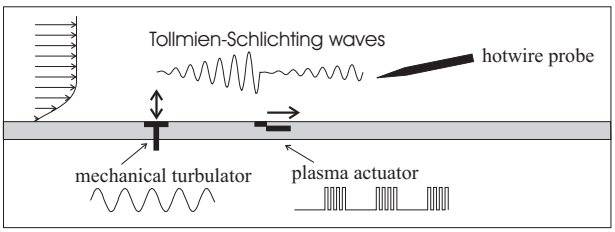


Figure 6: Details of the actuator placement

most clearly seen in Figure 5; 2. The second effect is the thinning of the boundary layer by the actuators, which leads to lower local Reynolds numbers. The actuators separate the local Reynolds number and the critical Reynolds number which leads to the delay of transition.

# 3 Pulsed Plasma Actuators

In the following section only one single control actuator is operated in pulsed mode to counteract the TS waves directly. This principle has been suggested by [18]. Particularly the cancellation of TS waves using zero-net mass flows through slits in the surfaces have proven very successful. These suction and blowing actuators have been applied by [2], [6] and [17]. Using numerical simulations [1] demonstrates the opposition control of TS waves by wall-parallel Lorentz forces. To achieve a wave cancellation, it is necessary to adjust the frequency and the amplitude of the actuator signal and to adjust the phase shift between the waves and the actuation signal. In this work the disturbances leading to the Tollmien-Schlichting waves are again acoustical excited using a vibrating surface driven by a electromagnetic actuator. Figure 6 shows a sketch of the two actuators and the measurement position. A software signal generator allows the electromagnetic actuator of the vibrating surface and the plasma actuator to be operated at the same frequency and with a specific phase shift between them.

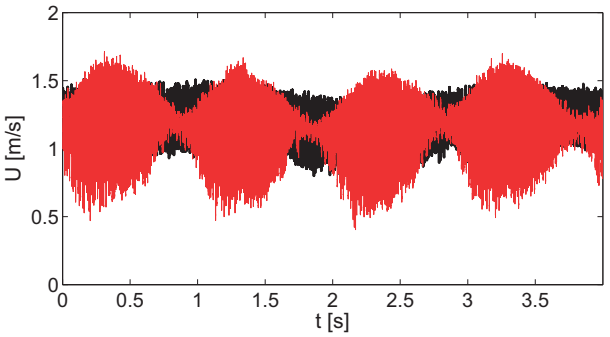


Figure 7: Time series of the amplitudes with (red) and without (black) actuation

The control actuator is positioned $100mm$ downstream of the vibrating surface. The vibrating surface excites oscillations in the boundary layer that grow as they travel downstream. All presented results have been achieved using the same signal amplitude for the electromagnetic actuator. The result of the excitation and attenuation is recorded $90mm$ downstream of the control actuator. This position was chosen to allow a strong downstream amplification of the waves without control and to allow enough time for a complete interaction of the control force with the waves. The velocity and turbulence profiles as well as the time traces and frequency spectra are measured using a hot-wire probe.

## 3.1 Superposition of Tollmien-Schlichting Waves

The frequency of the mechanical actuator is $f_{turb} = 110Hz$, which has been shown to be the frequency leading to the strongest amplification of the disturbances. If a control actuator is placed $100mm$ further downstream, depending on the phase shift $\Phi$ between the operating signals of the mechanical and the control actuator, there can be either an amplification or attenuation of the oscillations. A simple method to get a quick overview about the effect of different phase shifts is to operate both actuators at slightly different frequencies. Therefore the operating voltage of the control actuator is modulated with a square wave of $50\%$ duty cycle (DC) at a frequency of $f_{cont} = 111Hz$ to achieve a pulsed force production at this frequency. The plasma generating fre-

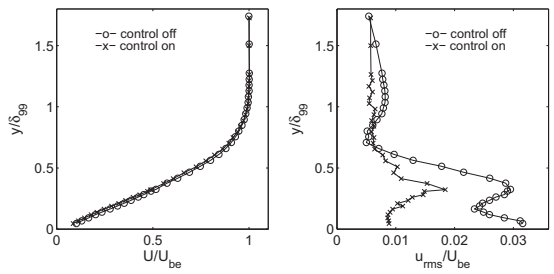


Figure 8: With and without wave cancellation

quency is $8kHz$ and the operating voltage is $7kV_{pp}$. The frequency difference of $\Delta f = 1Hz$ between excitation and modulation frequency of the plasma-actuator force generates a beat frequency of $f_{beat} = 1Hz$ in the flow, which leads to a continuously varying phase shift between both actuators. The resulting velocity fluctuations have been measured with a hot-wire probe $90mm$ further downstream of the control actuator at a height of $y = 1mm$. Figure 7 shows the comparison of the time traces of the velocities at this position: in black without the control actuator working and in red the modulated signal with both actuators. The black curve has a constant amplitude of $0.15m/s$. The mean value changes slightly due to small changes in the free-stream velocity $U_\infty$. The red curve denotes the superposition of the perturbations excited by the pulsed control actuator with the Tollmien-Schlichting waves excited by the vibrating surface. Depending on the phase shift, the oscillation is strongly amplified or attenuated to very small amplitudes.

### 3.2 Active Cancellation of Tollmien-Schlichting Waves

In the previous section the phase relation between both actuators was changed periodically in time. The phase shift in this section has a constant value of $\Phi = 220°$, which has been observed to be most effective for wave cancellation in this configuration. Since this phase value determines only the phase difference between the operating signal of the vibrating surface and the modulation of the plasma-actuator body force, this value cannot directly be interpreted in a fluid mechanical sense. The wavelength of the excited TS waves has not been determined experimentally. It can be assumed from [16] that the waves travel at approximately one third of the free stream velocity, which varies between the excitation and the control actuator due to the adverse pressure gradient. These uncertainties make

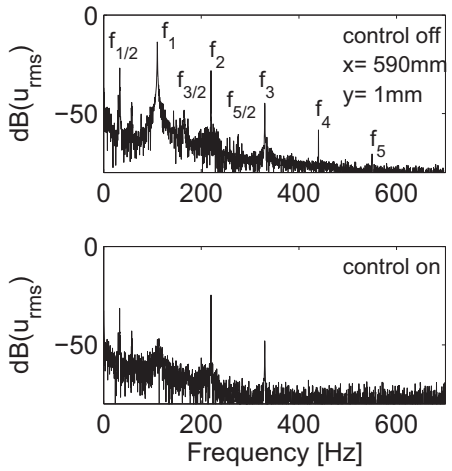


Figure 9: Power spectra densities at y=1mm

a fluid mechanical interpretation of the value of the phase shift misleading, since the interaction of the wave with the body force strongly depends on a precise adjustment of the local phase relation [10].

Figure 8 shows velocity and turbulence profiles $90mm$ downstream of the control actuator. The curves marked with circles show the uncontrolled laminar boundary layer. If the control actuator is operated at the same frequency the waves are cancelled considerably, as seen in the curve marked with crosses shows. The typical features of a TS-profile are no longer present. Overall the amplitudes of the oscillations are damped to values of $20 - 30\%$ of the uncontrolled boundary layer.

Figure 9 gives more detailed information about the frequency content and the shape of the fluctuations with and without control. The velocity fluctuations at the excitation frequency could be reduced significantly, while fluctuations of the two higher modes remain unchanged and the highest modes disappear. The data is measured at $x = 590mm$ and at the height $y = 1mm$.

## 4 Closed-Loop Control Circuits

Since the wave cancellation depends on a precise adjustment of several parameters, best results can only be obtained with a closed-loop control circuit that gains information about the cancellation results from a sensor. Two different approaches for the development of control circuits have been applied in this work.

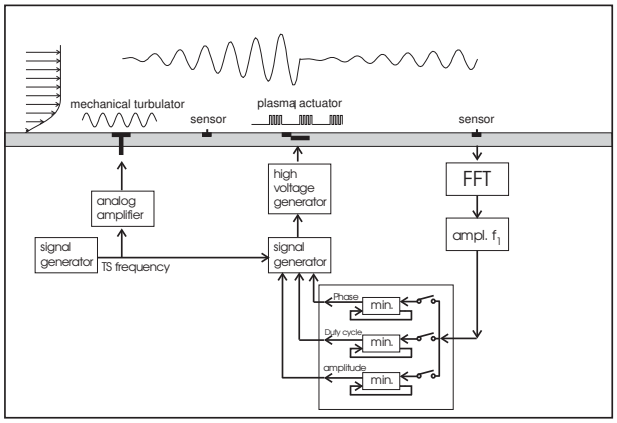


(a) First generation closed-loop control circuit.

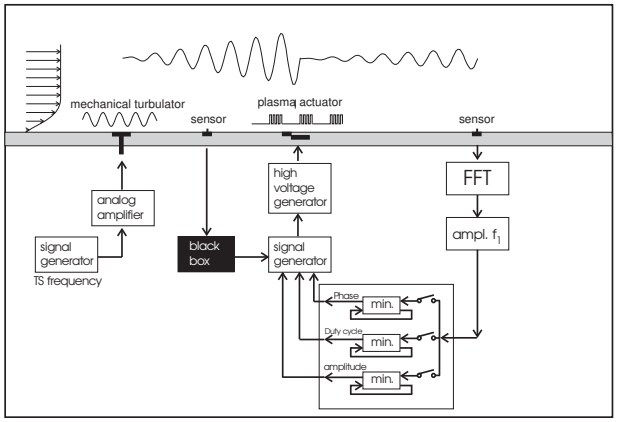


(b) Second generation closed-loop control circuit.

Figure 10: Scheme of the phase control circuit.

## 4.1 Phase Control

The first circuit presented here is a rather simple approach but it already shows the great potential of this technique. A principle sketch of the circuit is given in Figure 10(a). The TS waves are artificially excited by the vibrating surface. The waves travel downstream and interfere with the control-actuator force. The result of the interaction is recorded with a hot-film sensor downstream of the actuator. In each cycle of the control-loop the circuit changes slightly the value of one of the parameters, such as the phase, the duty cycle or the force amplitude. The resulting amplitude of the waves is compared with the one from the previous cycle. The control circuit determines if the previous step yielded an improvement or not. If yes, the next parameter change will be in the same direction and vice versa. A minimum of the amplitude is sought for each considered parameter.

This simple circuit can only control one parameter at a time. However, after several cycles the control circuit can switch between the control of different parameters. In the presented version the control circuit alternates between the control of the phase difference between the excitation and the control actuator and the duty cycle of the actuation. The step size of the parameter changes per cycle is depending on the actual amplitude to enable the circuit to find the minimum quickly with large steps and to maintain the optimal cancellation using small step sizes. The operating voltage of $6kV_{pp}$ and the operating frequency of $8kHz$ are not controlled by the control circuit and were kept constant. The loop-frequency is set to $3Hz$. This frequency allows enough time for the parameter changes performed by the circuit to show an effect and to achieve a reasonable signal-to-noise ratio on the input signal for the circuit.

A result of this wave-cancellation control circuit is given in Figure 11. The plot at the top of Figure 11 shows the velocity of the wind tunnel. It is abruptly altered manually in several steps. The control circuit has to react on these changes of the external operation conditions and to readjust the controlled parameters. The second and third diagrams show the phase and the duty cycle, which are both controlled by the circuit. The bottom diagram shows the amplitude of the waves measured by the downstream sensor. The control circuit is activated at the time $t = 5\,\mathrm{s}$. Before that time the amplitude diagram shows the amplitude of the not influenced TS waves. Quickly after the activation a minimum of the amplitude is found by the automated adaption of the phase and the duty cycle. Each time the tunnel velocity is changed manually the amplitudes of the waves increases rapidly but the circuit reestab-

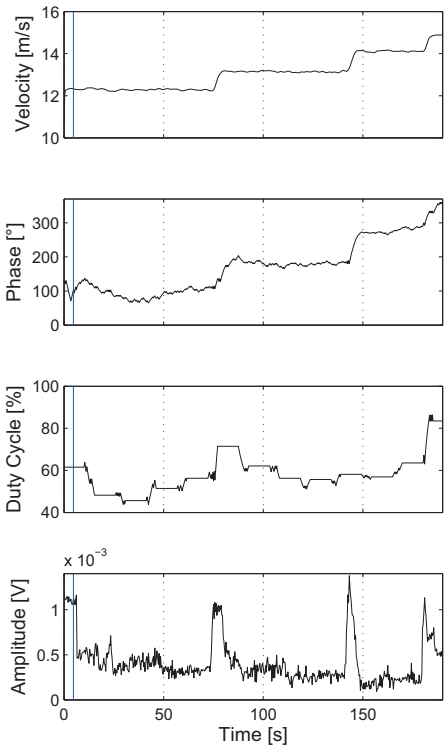


Figure 11: Cancellation results obtained with the phase control circuit.

lishes the low amplitudes by a precise wave cancellation. The fluctuations of the amplitude result from smaller changes that the control circuit makes and from noise in the flow. The noise leads to a number of wrong decisions of the control circuit and causes the slow convergence to the amplitude minimum. If the step sizes and the loop frequency of the control circuit are not chosen carefully these fluctuations cause the circuit to completely fail.

The presented results demonstrate the large potential of a closed-loop regulation in combination with plasma actuators. However, the frequency for the control-actuator operation could not be derived from measurements and hat to be taken directly from the signal generator of the wave excitation. This was necessary due to a bad signal-to-noise ratio of the upstream sensor and due to too slow hardware. In the next section another approach has been followed to address that problem and to develop a control circuit that is completely independent of such passed-in information.

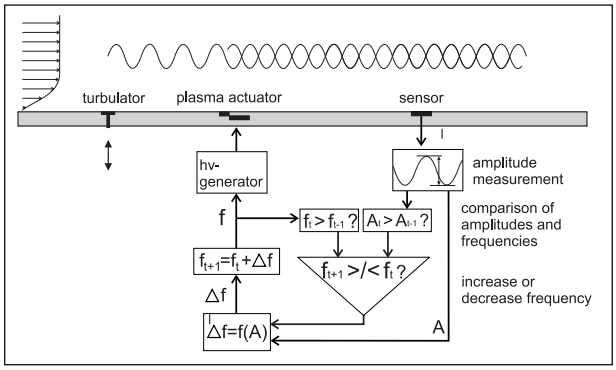


Figure 12: Scheme of the frequency control circuit.

## 4.2 Frequency Control

In Section 3.1 it has been shown that the wave cancellation is just a superposition of two oscillations, yielding constructive or destructive interference depending on the phase shift between both signals. Figure 7 shows the appearance of a beat frequency when the excitation and the control actuators are not operated at the same frequency. Therefore the idea of the development of the second control circuit is to capture the minimum of this beat-signal by precisely adjusting the modulation frequency $f_m$ of the control actuator. Once the modulation frequency of the control actuator $f_m$ matches the frequency of the Tollmien-Schlichting waves precisely, the beat disappears. Depending on the phase shift between both signals an increased or decreased amplitude of the TS waves will be detected by the downstream sensor. If now the modulation frequency is again detuned slightly, the beat will start again and the phase relation between the waves and the control-actuator signal starts to drift. A minimum of the measured amplitudes will occur and right in this moment the detuning has to be undone. By this means the destructive interference can be sought and adjusted.

Even though the operating principle of the control circuit is rather simple but the implementation of this idea in a successful experiment is not that simple. A functional sketch of the frequency-control circuit, developed by A. Güttler in [12], is shown in Figure 12.

Similar to the control circuit for the phase control in the previous section, this circuit changes the value of the controlled parameter, the modulation frequency, in each cycle of a loop. The waves are recorded by the downstream sensor and their amplitude is determined. Next the actual amplitude is compared with the amplitude of the previous cycle and the actual modulation frequency with the one before. Both information are needed to decide wether the last fre-

quency change yielded an improvement of the cancellation or not. Then the $\Delta f$ for the frequency of the next cycle is determined. The sign of the frequency change results from the previous decision and its value is dependent on the actual amplitude. It is necessary to make larger steps when the modulation frequency $f_m$ is rather different from the TS-wave frequency, whereas smaller steps are necessary to seek and maintain the destructive interference, when both frequencies a very close. The circuit works completely independent of any external information, such as the exact excitation frequency. The circuit doesn't even need an upstream sensor. For a quick tuning of the circuit it is advantageous if the frequency of the TS waves is known roughly. To determine the TS-frequency the circuit performs a Fast-Fourrier-Transformation (FFT) during one second prior to the activation of the control actuator. After this initial measurement the circuit can find the optimal parameters relatively quick. If the circuit fails to tune the frequency or if it looses the control of the TS waves, the sensor will detect large amplitudes. In that case the circuit resets itself by turning off the actuator and restarting with a FFT. Such a situation is shown in Figure 13. After $t = 50\,\mathrm{s}$ the control circuit makes several wrong decisions and looses control. At $t = 52\,\mathrm{s}$ the circuit resets itself and turns the actuator off. During the next second the time trace of the amplitude signal shows the amplitude of the non-influenced TS waves. Right before $t = 52\,\mathrm{s}$ the constructive interference can be observed. Very soon after the new FFT the circuit is tuned again and despite the rectangular modulation of the cancellation-body force quite large attenuation rates of $75\,\%$ can be obtained. Therefore further improvement is to be expected in future works when the modulation of the control actuators body force will be adapted to the sinusoidal modulation of the TS waves.

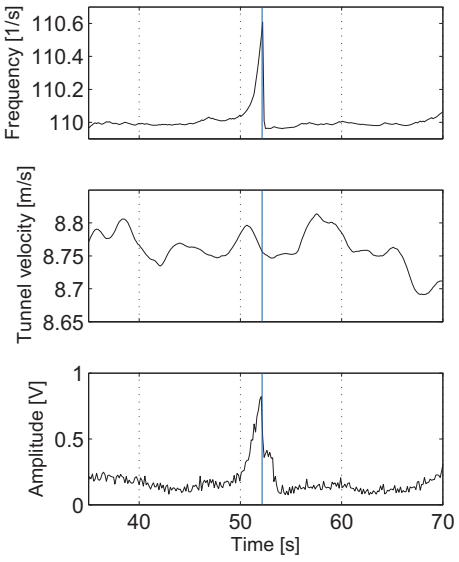


Figure 13: Cancellation results obtained with the frequency control circuit.

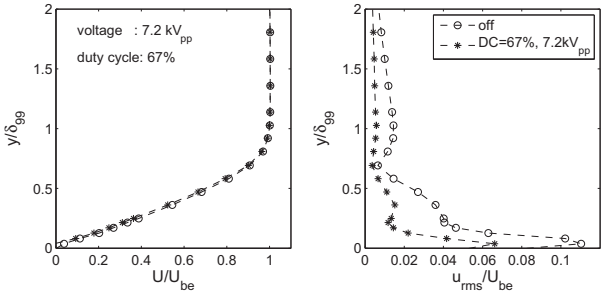


Figure 14: Velocity and turbulence profiles with optmized parameters: $E_{pl} = 7.2\,\mathrm{kV_{pp}}$ and $DC = 67\,\%$.

# 5 Delaying Transition Using Active Wave Cancellation

The delay of transition using the active-wave cancellation technique is a more demanding task than with the steadily operated plasma actuators, because the operation parameters of the cancelling actuator have to be adjusted precisely, as discussed above. A parameter configuration that is optimized for certain conditions does not yield the same results when the wind-tunnel velocity changes. A control circuit is necessary, as described in the previous section. Nevertheless also without a closed-loop control it was possible to demonstrate a mentionable delay of transition at a free-stream velocity of $8\,\mathrm{m/s}$, measured at the end of the test section. The experimental setup is the same as above. In this case the optimal duty cycle is again $DC = 67\,\%$ at an operating voltage of $E_{pl} = 7.2\,\mathrm{kV_{pp}}$ and an operating frequency of $f_{pl} = 8\,\mathrm{kHz}$. The modulation frequency is the same as the excitation frequency $f_m = 110\,\mathrm{Hz}$ and the phase shift between the control signal for the vibrating surface and the force modulation is again $Phi = 220$. Figure 14 shows the velocity profiles with and without control actuator working $90\,\mathrm{mm}$ downstream of the control actuator. The amplitude of the TS-wave is reduced significantly up to heights of twice the boundary-layer thickness $\delta_{99}$.

Using this parameter configuration the velocity profiles at several downstream positions have been measured for both cases to detect whether the point

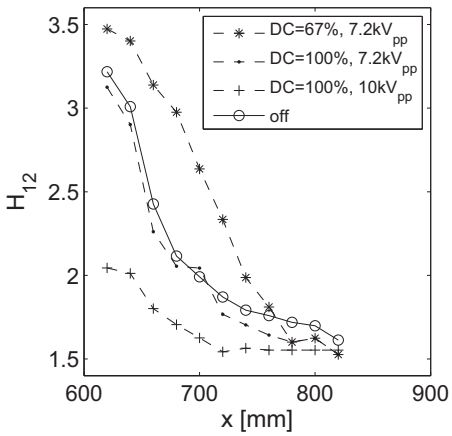


Figure 15: Shape-factor development and transition delay for pulsed and non-pulsed actuation.

of transition could be shifted or not. Figure 15 shows the shape factor developments of the velocity profiles along the x-direction. A delay of the transition by approximately $60\,\mathrm{mm}$ is clearly visible. This is about one third of the value achieved in the previous section with two steadily operated plasma actuators. However, the energy consumed here is approximately one order of magnitude smaller, as discussed in the next Section 6. To prove that the quality of the attenuation of the waves relays on the unsteady actuation, two further experiments have been conducted and their results are also included in Figure 15.

It has been shown in [10] that the wave cancellation with pulsed operation can yield better results than a steady actuation ($DC = 100\,\%$) at the same operating voltage. The same observation can be made here. Figure 16 shows the case with steady operation at an operating voltage of $E_{pl} = 7.2\,\mathrm{kV_{pp}}$. The amplitude of the TS-wave closed to the wall is significantly reduced but in comparison to the case shown in Figure 14 the amplitudes remain larger. Especially above the phase jump of the wave, the amplitudes are higher than in the pulsed case. The result of this attenuation is included in Figure 15 and does not show a delay of the point of transition. The reaction of the boundary layer is insignificant to the manipulation even though more energy is added to the flow.

The steady actuation at higher operating voltages has been shown to be a reliable method to attenuate perturbations. Therefore another experiment has been performed to prove the superiority in terms of low energy consumption of the active wave cancellation. Again the control actuator is operated in the continuous mode ($DC = 100\,\%$) but the operating voltage was increased to $E_{pl} = 10\,\mathrm{kV_{pp}}$ yielding a larger body force. The resulting profiles of the mean velocity and the fluctuations are shown in Figure 17. The velocity profile is clearly disturbed and deformed. Transition has been promoted, as the profile of the velocity fluctuations shows. The corresponding shape-factor development is also included in Figure 15. The steady actuation at the higher voltage promotes the transition in stead of delaying it.

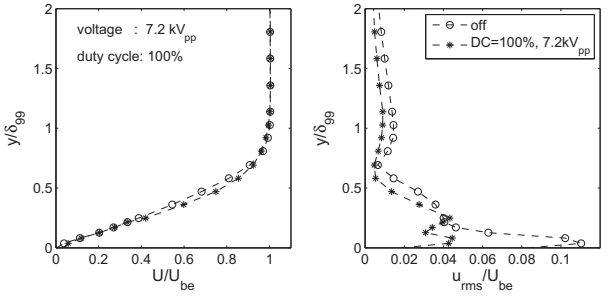


Figure 16: Velocity profiles and turbulence profiles with steady actuation at $E_{pl} = 7.2\,\mathrm{kV_{pp}}$ and $DC = 100\,\%$.

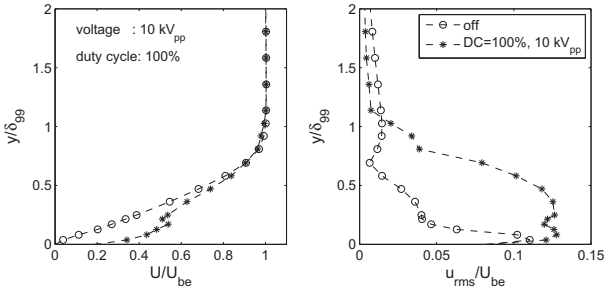


Figure 17: Velocity profiles and turbulence profiles with steady actuation at $E_{pl} = 10\,\mathrm{kV_{pp}}$ and $DC = 100\,\%$.

The discussed set of experiments prove the high efficiency of a precise pulsed operation in comparison to the steady operation. The transition can be delayed with much lower energy consumption. In this special configuration the pulsed actuation showed to be the only operation mode that can delay the laminar-to-turbulent transition.

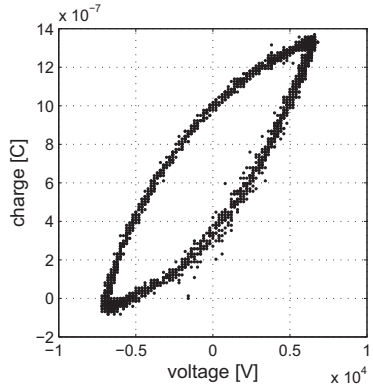


Figure 18: Voltage-charge plot.

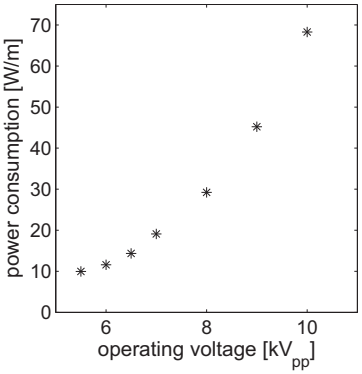


Figure 19: Power consumption of the plasma actuators as used in this work dependent on the operating voltage.

# 6 Pulsed vs. Steadily-Operated Plasma Actuators

## 6.1 Determining the Power Consumption of DBD Plasma Actuators

A reliable and accurate method to determine the power consumption is to integrate the current passing through the actuator in time using a capacitor. The voltage of the capacitor depends on the charge across it. This analog integration of the current catches all discharge pulses and yields a very accurate measurement of the charge that has passed through the actuator. The energy consumed by the actuator in one period of the HV-cycle can be determined by integrating the area inside a Lissajous Figure of a charge-vs.-voltage plot [14, 3, 4]. Multiplying by the frequency of the operating voltage yields the power dissipated by the actuator. The energy consumption of the plasma actuators used in this work has been determined using this method. An example for a charge-vs.-voltage plot is shown in Figure 18.

The power consumption at different operating voltages have been determined and the results results are plotted in Figure 19. The correlation between the dissipated power and the applied voltage follows a quadratic dependency as known from the literature [5, 15].

## 6.2 Comparison of the Consumed Power

The power consumption of the direct cancellation of TS waves is far lower than by indirect attenuation of perturbations by changing the velocity profile, as

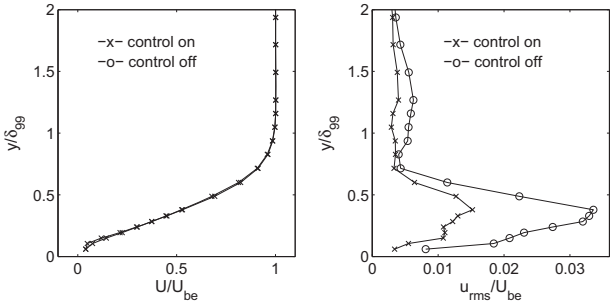


Figure 20: Velocity- and turbulence profiles with and without steady actuation ($x = 550mm$, $DC_{pl} = 100\%$, $E_pl = 10kV_{pp}$)

presented in the first part of this work. Figure 20 shows results obtained using steady actuation. In this figure we find similar amplitudes for the case without control and similar cancellation rates with the control actuators working, as achieved using the pulsed actuation shown in Figure 8.

The energy consumed by the non-pulsed plasma actuator as used in Figure 20 has been determined to be $68.3\,W$ per meter actuator length. In comparison to that, the actuator consumes only $11.6\,W$ per meter when it is operated at $E_{pl} = 6kV_{pp}$, as used for the active wave cancellation. Additionally, the actuator has been operated in pulsed mode at a duty cycle of $DC_{pl} = 70\%$ yielding a power consumption for the active wave cancellation of $8.1\,W$ per meter of actuator length. This is only $12\%$ of the energy consumed by the steady perturbation attenuation, while the amount of turbulence left in the boundary layer is nearly the same for both cancellation principles.

# 7 Conclusions

In previous investigations of DBD plasma actuators in laminar boundary layers it was demonstrated that plasma actuators can be used as switchable transition trips that can easily promote the transition. In this manuscript it could be shown that plasma actuators in a laminar boundary layer do not necessarily promote transition, but can even be applied to delay transition. Two methods using steadily operated and pulsed actuators have been successfully applied. Even though the steady operation consumes considerably more energy than the active wave cancellation, it is by far more robust and easier to apply. The results show the great potential of Dielectric Barrier Discharge (DBD) Actuators for flow-control applications in laminar boundary layers. Further efforts to develop such applications incorporating plasma actuators will only be made if interesting technical applications are to be expected. The authors have attempted to demonstrate one such application.

# References


[1] T. Albrecht, H. Metzkes, R. Grundmann, G. Mutschke, G. Gerbeth, Tollmien-Schlichting wave damping by a streamwise oscillating Lorentz force, Magnetohydrodynamics 44 (3) (2008) 205–222.

[2] S. Biringen, Active control of transition by periodic suction-blowing, Physics of Fluids 27 (1984) 1345.

[3] G. Borcia, C. Anderson, N. Brown, Dielectric barrier discharge for surface treatment: application to selected polymers in film and fibre form, Plasma Sources Sci. Technol. 12 (2003) 335–344.

[4] Z. Falkenstein, J. Coogan, Microdischarge behaviour in the silent discharge of nitrogen oxygen and water air mixtures, Applied Physics 30 (1997) 817–825.

[5] M. Forte, J. Jolibois, J. Pons, E. Moreau, G. Touchard, M. Cazalens, Optimization of a dielectric barrier discharge actuator by stationary and non-stationary measurements of the induced flow velocity - application to airflow control, Experiments in Fluids 43 (6) (2007) 917–928.

[6] M. Gaster, Active control of boundary layer instabilities using MEMS, Current Science 79 (2000) 774.

[7] S. Grundmann, Transition Control using Dielectric Barrier Discharge Plasma Actuators, Shaker Verlag, ISBN 978-3-8322-7587-7, 2008.

[8] S. Grundmann, T. Klumpp, C. Tropea, Stabilizing a laminar boundary layer using plasma actuators, in: Proceedings of the 25th International Congress of the Aeronautical Sciences, No. ID 255, Hamburg 2006.

[9] S. Grundmann, C. Tropea, Experimental transition delay using glow-discharge plasma actuators, Experiments in Fluids 42 No.4 (2007) 653–657.

[10] S. Grundmann, C. Tropea, Active cancellation of artificially introduced tollmien-Schlichting waves using plasma actuators, Experiments in Fluids 44 No.5 (2008) 795–806.

[11] S. Grundmann, C. Tropea, Experimental damping of boundary-layer oscillatoins using plasma actuators, International Journal of Heat and Fluid Flow In Press (2009) DOI: 10.1016/j.ijheatfluidflow.2009.03.004.

[12] A. Güttler, Auslegung, Umsetzung und Erprobung verschiedener Regelkonzepte zur aktiven Dämpfung von Tollmien-Schlichting Wellen mit Hilfe von Plasma Aktuatoren, Bachelor's Thesis, Technische Universität Darmstadt.

[13] E. Moreau, Airflow control by non-thermal plasma actuators, Journal of Physics D: Applied Physics 40 (2007) 605–636.

[14] G. Nersisyan, W. Graham, Characterization of a dielectric barrier discharge operating in an open reactor with flowing helium, Plasma Sources Sci. Technol. 13 (2004) 582–587.

[15] J. Roth, X. Dai, Optimization of the aerodynamic plasma actuator as an electrohydrodynamic (EHD) electrical device, AIAA Aerospace Sciences Meeting and Exhibit.

[16] H. Schlichting, Boundary-Layer Theory, Verlag G.Braun, 1982.

[17] D. Sturzebecher, W. Nitsche, Active cancellation of Tollmien-Schlichting instabilities on a wing using multi-channel sensor actuator systems, Heat and Fluid Flow 24(4) (2003) 572–583.

[18] O. Wehrmann, Tollmien-Schlichting waves under the influence of a flexible wall, Physics of Fluids 8 (1965) 1389.